



CHORUS

This is the accepted manuscript made available via CHORUS. The article has been published as:

Anomalous photoluminescence Stokes shift in CdSe nanoparticle and carbon nanotube hybrids

Austin J. Akey, Chenguang Lu, Lijun Wu, Yimei Zhu, and Irving P. Herman

Phys. Rev. B **85**, 045404 — Published 3 January 2012

DOI: [10.1103/PhysRevB.85.045404](https://doi.org/10.1103/PhysRevB.85.045404)

Anomalous Photoluminescence Stokes Shift in CdSe Nanoparticle/Carbon Nanotube Hybrids

*Austin J. Akey,^{†1} Chenguang Lu,^{†1} Lijun Wu,² Yimei Zhu,² and Irving P. Herman^{*1}*

¹ Department of Applied Physics and Applied Mathematics

Columbia University

New York, NY 10027

² Department of Condensed Matter Physics, Brookhaven National Laboratory

Upton, NY 11973

[†] *These authors contributed equally*

** Corresponding author*

Abstract

A very large decrease in the Stokes shift in CdSe nanoparticle photoluminescence is seen from hybrid materials in which the nanoparticles are attached to single-walled carbon nanotubes after pyridine treatment relative to unbound nanoparticles capped by pyridine. This is observed particularly for very small nanoparticles, for hybrids composed of core-only and core-shell nanoparticles, and for hybrids made with bundles of mixtures of semiconducting and metallic nanotubes or with semiconducting nanotubes only, and is likely due to fast Förster resonance energy transfer (FRET) from the nanoparticles to the nanotubes. A simple model demonstrates the plausibility of the hot luminescence explanation of this decreased Stokes shift.

I. Introduction

Hybrid nanomaterials composed of CdSe quantum dot colloidal nanoparticles (NPs) and single-walled carbon nanotubes (SWNTs) are attracting great interest for their potential light-harvesting properties¹⁻⁷. Many attachment methods for creating the hybrids involve functionalizing the nanotubes at defect sites, which can change the electronic and mechanical structure of the nanotube, introducing a linker molecule between the nanotube and nanoparticle, or growing nanoparticles on nanotube sidewalls^{3,7}. We have previously demonstrated an attachment method that does not require nanotube functionalization⁸. Unusual nanoparticle photoluminescence in these hybrids is reported here that is believed to arise from excitation transfer within the hybrid, and this could be of importance in photovoltaic applications.

II. Sample Preparation and Characterization

The synthesis of CdSe nanoparticles and CdSe/ZnS core-shell nanoparticles is described in the Supplemental Information. CdSe nanoparticle/single-walled carbon nanotube hybrids were prepared following a previously published technique^{8,9}. CdSe nanoparticles were precipitated from toluene solution using methanol, sonicated in pyridine for 4 h, and then precipitated using hexane. This process was repeated until a transparent solution of nanoparticles in pyridine was produced, indicating that the nanoparticles were fully capped with pyridine. Purified SWNT (either HiPCO following acid and thermal treatment to remove remaining catalyst particles or arc-discharge purchased already-purified from NanoIntegris) were added to the nanoparticle solution, and sonicated together for 1 h. The resulting hybrids were then washed with pyridine to remove unbound particles. Nanoparticle sizes ranged from 1.4 nm radius to 3.4 nm radius, and included both CdSe nanoparticles and CdSe/ZnS core-shell nanoparticles (~3 ZnS layers). Nanoparticles, nanotubes and hybrids were characterized by high resolution

transmission electron microscopy (HRTEM), thermal gravimetric analysis (TGA), and visible absorption and photoluminescence (PL) spectroscopies. The hybrids were analyzed by an ultrahigh resolution TEM/STEM (JEOL 2200MCO) at Brookhaven National Laboratory. The instrument, equipped with two aberration correctors and an in-column Omega filter, is usually operated at 200 kV, but is optimized at 80 kV for imaging light elements, such as carbon. The visible absorption spectra were acquired for solutions of hybrids in pyridine using a UV-Vis spectrometer. Steady-state photoluminescence measurements were performed using a cw argon-ion laser, interfaced with a confocal microscope (3 μm spot size), spectrometer, and CCD array detector. PL from samples either suspended in pyridine or drycast on cleaned silicon wafers was measured with excitation at 514.5 nm or 488.0 nm (1 mW).

Figure 1 shows high-resolution TEM micrographs of the hybrids made with these HiPCO SWNTs. Monodisperse colloidal CdSe nanoparticles were directly attached to the nanotubes, which were usually in bundles. NPs are seen to attach only to the bundles of SWNTs, although they are sometimes clustered next to each other on the nanotubes. In previous work⁸, we showed that the absorption spectrum of the hybrids is a linear combination of the absorption spectra of the components (Fig. S1 in Supplemental Information). Extremely fast electronic or dipole-dipole coupling, which would reduce the effect of quantum confinement, and polarization effects, resulting in an increase in the dielectric constant around the NP, would cause a red-shift in the position of the first exciton peak. These effects are not observed in our samples.

III. Optical Measurements

In Fig. 2, PL spectra from the hybrids formed using HiPCO SWNTs are compared to the PL spectra from the unbound nanoparticles, which had been capped with pyridine, and to NP absorption (for an NP solution). The magnitudes of the Stokes shifts from the first exciton

features in the absorption spectra to the PL peaks of the unbound NPs are consistent with those previously reported¹⁰⁻¹² and these shifts generally increase with smaller NP radius^{13, 14} (Fig. S2 in Supplemental Information). The PL spectra peak energies are seen to be the same for solutions and powders of the unbound NPs and also the same for solutions and powders of the hybrids. The intensity of the hybrid PL signal in the NP emission region is comparable to the resonant Raman peaks¹⁵ from the carbon nanotubes, and is much smaller than that observed from the unbound nanoparticles. The linewidths of the hybrid PL peaks are comparable to those from unbound nanoparticles. The PL spectra are the same for excitation at 514.5 nm (Fig. 2) and 488 nm. These results were highly repeatable, across all measured nanoparticle types and sizes; variations in nanotube attachment between individual SWNTs were averaged out by the size of the laser spot, and by measurements in solution phase. Measurements of the SWNTs alone resulted in only the expected SWNT Raman spectra, both in dry samples and pyridine suspension.

Figure 2 shows that the Stokes shift (the difference between the energy of the first exciton peak in absorption of the unbound nanoparticles and energy of the PL peak of the unbound nanoparticles and hybrids) is smaller for the bound hybrid nanoparticles than for the unbound ones. This difference (i.e., the decrease in the Stokes shift) increases with smaller NP radius (Fig. 3). Moreover, the Stokes shift decreases in the hybrids with smaller nanoparticle radius, whereas it generally increases in unbound NPs (Fig. S2 Supplemental Information). For example, for 3.4 nm radius nanoparticles the Stokes shift is 60 meV for unbound NPs and 50 meV for the hybrids, so the hybrid Stokes shift is smaller by 10 meV (Fig. 2b). In contrast, for 1.4 nm radius nanoparticles the Stokes shift is 158 meV for unbound NPs and 8 meV for the hybrids, so the hybrid Stokes shift is smaller by 150 meV (Fig. 2a). Figure 4 shows that CdSe/ZnS core shell NPs (1.6 nm core radius) and hybrids composed of them and SWNTs

exhibit a reduction in the Stokes shift for the hybrid, which corresponds to that seen for CdSe core-only NPs.

Single-wavelength ultrafast PL measurements of unbound CdSe NPs and NP/HiPCO SWNT hybrids suspended in pyridine were made at the Center for Functional Nanomaterials at Brookhaven National Laboratory, using Ti:Sapphire laser excitation (455 nm, 200 fs pulse width, power 1 mW) and detection with a Picoharp 300 system (4 psec time resolution, after an initial delay of 45 ps after excitation). The time dependence of PL at 577 nm in Fig. 5 shows that NP/SWNT coupling is much faster than radiative and nonradiative decay in the unbound NPs, and shorter than the instrument 45 ps initial delay time in data acquisition. No evidence of unbound NPs in the hybrid sample is seen.

The HiPCO nanotubes used to form the hybrids consist of approximately 1/3 metallic and 2/3 semiconducting SWNTs, 0.9-1.2 nm in diameter, so the bundles of nanotubes in the hybrids are expected to contain both semiconducting and metallic SWNTs. In order to distinguish the behavior of the different nanotube types, hybrids were also formed in the same manner using arc discharge nanotubes separated by density gradient ultracentrifugation¹⁶ to isolate semiconducting or metallic SWNTs (both of >99% purity and bundled) (NanoIntegris). TEM (Fig. S3 in Supplemental Information) shows that NP attachment to both types of SWNTs looks similar to that for the HiPCO nanotubes, so NP decoration appears to be the same for semiconducting and metallic nanotubes, as well as being the same for the smaller HiPCO nanotubes (0.9-1.2 nm) and larger arc discharge nanotubes (1.2-1.5 nm). The semiconducting-nanotube hybrids have essentially the same PL spectra as the HiPCO hybrids, with the same Stokes shifts, absorption peaks and linewidths (Fig. 6), although their Raman spectra are slightly different due to their different chirality and diameter distribution¹⁵. The metallic-nanotube hybrids, however, have PL spectral features that peak at an energy just below or (in some cases) slightly higher than that of

the NP first exciton absorption peak, and are much weaker than the PL of semiconductor-nanotube hybrids (Fig. 6).

IV. Discussion

After carrier creation by illumination, carrier equilibration occurs very quickly (< 200 fs)¹⁷ in the NPs, and is followed by NP carrier energy relaxation¹⁸⁻²⁰, NP radiative decay^{13, 21-24}, and NP nonradiative decay²¹; in the hybrids, there is also coupling from the NP to SWNT. The Stokes shift in CdSe NP PL is thought to arise from radiative decay from either dark to bright exciton states during and after electronic level relaxation or from lower energy levels after interactions with phonons, or from both²⁵⁻²⁷. Coupling from a bound NP (acting as donor) to the SWNT (as acceptor) could be due to the dipole-dipole coupling of Förster resonance energy transfer (FRET) and/or charge transfer, including exciton transfer, or transfer of electrons and/or holes²⁸⁻³¹. When this coupling is comparable or fast compared to NP relaxation, radiative, and intra-nanoparticle nonradiative decay, weaker overall NP PL emission is expected and the PL spectrum is expected to be blue shifted relative to that from unbound NPs; this represents a “snapshot” of PL at the early stages of emission from unbound NPs, or “hot luminescence.” Coupling between adjacent NPs on a given SWNT (as in Fig. 1) would instead lead to a red shift in PL due to FRET between the NPs or the loss of quantum confinement, and consequently is not significant here³².

The explicit dependence of the Stokes shift with NP radius in the hybrid could be affected by the distance between the centers of the bound NP and SWNT for FRET; changes in band alignment due to changes in the NP conduction and valence band levels, energy barriers in hybrid binding, and surface contact areas for charge transfer; and the explicit dependence of relaxation rates on NP radius.

For the hybrid point dipole-linear dipole geometry, the rate of FRET varies as $1/r^5$, where r is the separation of the centers of the bound NP and SWNT. The actual FRET rate would not scale exactly as $1/r^5$ at these small NP/SWNT separations because the dipole-dipole coupling approximation breaks down²⁸. Also, since the excitons may be localized near the surface, the exact definition of r may need to be modified. Potential charge transfer would be sensitive to the precise structure of the NP/SWNT binding. The NP and SWNT band alignment^{5, 33} suggests that electron transfer would be possible, and likely hole (and exciton) transfer would not be possible. There could be a barrier to charge transfer, perhaps due to the presence of pyridine on the nanoparticle surface (if in fact it remains bound to the nanoparticle). CdSe NP and CdSe/ZnS core-shell NP hybrids have similar decreased Stokes shifts in the hybrid (Fig. 4). Because the ZnS layer would serve as a barrier for electron and hole transfer, this suggests that charge transfer is not the major NP-SWNT coupling mechanism here.

The small or “negative” Stokes shift and very weak PL characteristic of the metallic-nanotube hybrids may be due to FRET and charge coupling from the attached nanoparticles that are much faster than to the semiconductor nanotubes. NP PL would then occur only from levels near or above the absorption edge or from the smaller NPs in the hybrids. In the hybrids formed with the HiPCO SWNT mixtures, the observed PL is likely from hybrids with the nanoparticles attached to a semiconducting SWNT; the PL is expected to be very weak in those hybrids with nanoparticles attached to a metallic SWNT and in those with NPs bound to a semiconductor SWNT in a bundle containing many metallic tubes.

A. Photoluminescence Model

The plausibility of the hypothesis that FRET from the NP to the SWNT causes the decreased Stokes shift in the hybrids is examined in two alternative simple energy-level models

that mimic two potential modes of relaxation leading to PL in unbound and hybrid NPs: the steady-state “phonon model” and the local equilibrium “electronic state model”. In both models, there is one ground state (level $i = 0$ with energy $E = 0$, with population density n_0) and then a series of equally-spaced excited levels ($i = 1, 2, 3, \dots$, with respective densities n_i), with spacing Δ (Fig. 7). The lowest excited energy level is E_1 , corresponding to an excited electronic state (and which is usually near the PL energy, aside from the spectral broadening and phonon Stokes shift considerations described below). Because of the Stokes shift, the first exciton peak in absorption corresponds to a state $i_{\text{abs}} (>1)$, which is at energy E_{abs} . Level i_{exc} is directly excited by the cw laser, by photons with energy E_{exc} .

The relaxation rates are largely determined using published experimental rates, which vary with NP size^{18,21}. Rates are assumed to be independent of level (except as described below). The PL spectrum comes from radiative decay from each excited state to the ground state, each a Gaussian spectrum with a width set to reproduce the NP PL spectral profile. Model Stokes shifts in unbound NPs are compared to the measurements (which are consistent with published results), and then NP-SWNT coupling is added. There is no back-coupling from the SWNT to NP in the model.

The PL spectrum comes from radiative decay in the NP (of radius r , in nm) from each excited state i [$\gamma_{\text{rad},i}(r)$] to the ground state, with each a Gaussian profile centered about E_i , with width ϵ . The PL emission rate at energy E (photons per unit time and volume) is:

$$I_{\text{PL}}(E) = \sum_{i=1}^{i_{\text{exc}}} \gamma_{\text{rad},i}(r) n_i(E_i) S(E - E'_i, \epsilon) \quad (1)$$

Although an explicit dependence of radiative decay on level i is indicated here, it is assumed to be independent of i (except as noted below). S is a normalized Gaussian centered about the

emitting level i , with emission at E'_i with full width at the $1/e$ points of ε . In the electronic state model $E'_i = E_i$ and in the phonon model it is modified, $E'_i = E_i + (1 - 1/f)\Delta(i_{\text{abs}} - i)$, as described below; f is defined below. ε reflects the inhomogeneity of nanoparticle sizes and is chosen to reproduce the observed NP PL spectral profiles. Model Stokes shifts in NP PL are compared to the experimental measurements for unbound NPs and then, with NP-SWNT coupling included, for the hybrids.

Relaxation Modes and Rates

Equilibration of excited electronic states is very rapid¹⁷, within 200 fs; this is very important in the electronic state model. State-to-state relaxation in the excited state ladder occurs at a rate γ_{relax} , corresponding to the energy relaxation rate in Ref. 18 (γ^E) divided by the energy separation of the states Δ :

$$\gamma_{\text{relax}}(r) = (2.6316/r)^{2.6}/\Delta \quad (2)$$

All rates are in ps^{-1} and energies, such as Δ , in meV. The nonradiative and radiative relaxation rates are²¹:

$$\gamma_{\text{nonrad}}(r) = e^{-1.5E_{\text{abs}} + 20.83} \quad (3)$$

$$\gamma_{\text{rad}}(r) = \gamma_{\text{rad}}(r = 1 \text{ nm}) r^{-3} \quad (4)$$

where E_{abs} depends on r , and $\gamma_{\text{rad}}(r = 1 \text{ nm}) = 5 \times 10^{-5} \text{ ps}^{-1}$. In most cases, it is assumed that these rates are independent of i (≥ 1). Coupling from the NP to the SWNT in the hybrid by FRET

occurs at a rate^{28, 29}

$$\gamma_{\text{coupling}}(r, \rho, R) = \gamma_{\text{rad}}(r)[R_0/(r + \rho + R)]^5 \quad (5)$$

where ρ is the radius of the nanotube, R is the distance between the closest NP and SWNT surfaces, and R_0 is the distance between the centers of the NP and SWNT at which FRET has an efficiency of 50%. This expression is appropriate for transfer between a point “dipole” and an infinitely long linear “dipole” in the dipole-dipole coupling limit ($R \gg r + \rho$) and is used here even for $R < r + \rho$; this assumption is re-examined below^{26, 28, 29}. This rate is also assumed to be independent of i (≥ 1). The details of the spectral overlap between the donor NP and acceptor SWNT are ignored, since even the purified nanotube samples contain a large range of different nanotube chiralities with different absorption spectra.

The Phonon Model

In this model the excited states describe different levels of vibrational/phonon excitation in an excited electronic state. The energy difference between i_{abs} and any emitting level i is assumed to account for a given fraction f of the entire Stokes shift in the unbound NPs. (In molecular PL there are contributions to the Stokes shift in both excited and ground electronic states.) This is included in Eq. 1 by having emission from level i occur at the lower energy $E'_i = E_i + (1 - 1/f)\Delta(i_{\text{abs}} - i)$. The population of excited states is determined by a series of rate equations that give the steady-state populations balancing excitation from level 0 to a resonant excited state and subsequent relaxation, using γ_{relax} , γ_{nonrad} , γ_{rad} , and, for the hybrid only, γ_{coupling} . Carrier equilibration is not explicit in this model.

The population densities of the levels are given by:

$$n_{i_{exc}} = (\alpha I / E_{exc}) (1 / \Gamma_{i_{exc}}) \quad (6)$$

$$n_i = (\gamma_{relax,i+1} / \Gamma_i) n_{i+1} \quad (7)$$

where I is the laser intensity, α is the absorption coefficient, and

$$\Gamma_i = \gamma_{relax,i}(r) + \gamma_{nonrad,i}(r) + \gamma_{rad,i}(r) + \gamma_{coupling,i}(r) \quad (8)$$

where $\gamma_{coupling}$ is zero for unbound NPs and γ_{relax} is zero for $i = 1$ (the lowest excited level). PL emission is described using Eq. 1.

Figures 3 and S2 plot the phonon model predictions for the Stokes shifts of unbound NPs and hybrids, and their differences, as a function of particle radius, using $f = 0.5$ (and other conditions described below); this demonstrates the plausibility of this model in simulating the Stokes shifts in the unbound NPs and hybrids. Figure S4 shows that the agreement improves with smaller f (0.25), but we use $f = 0.5$ as the base case because roughly half of this Stokes shift is usually in the vibrational manifold of the excited electronic state²⁶ and the fits for the NP and hybrids Stokes shifts are best for $f = 0.5$ (Fig. S5). To reproduce the slight increase in Stokes shift with radius ($> \sim 2.5$ nm) and also (independent of this) to model the shift in the hybrids and the relative shift between unbound and hybrids NPs, the energy relaxation rates need to be faster than the values from Ref. 18. In the base case model, called “fast energy relaxation” in the figures, the energy relaxation rates for the levels at and above band-edge ($\geq i_{abs}$) need to be at least $4\times$ the rate from Ref. 18 and are set at $4\times$ this rate, and the average energy relaxation rate is then faster than the experimental value by a factor of ~ 3.5 . Models with linear and exponential

increases in relaxation rate with i lead to similar results. In particular, the relaxation rate in a harmonic oscillator should vary as the lower mode number plus one, which would be i here, so γ_{relax} would be proportional to i . With these linear or exponential dependences, average energy relaxation rates are also faster than the experimental value, specifically $\sim 2.5\times$ faster for the linear dependence. Such fast energy relaxation is also needed to obtain the same (unbound) NP Stokes shift with 488 and 514.5 nm excitation.

A Gaussian width ϵ in Eq. 1 of 122 meV reproduces observations well. The results are largely insensitive to the level spacing Δ over the range tested from 1 meV to 100 meV, which is not surprising since an energy rate of relaxation is used in the model. The model results are given in Figs. 3 and S5 for a spacing of 1 meV. For larger spacings there are oscillations about this envelope, as is seen in Fig. S6 for $\Delta = 25.4$ meV, the CdSe LO phonon energy. Model results are also the same with a decreasing level spacing with increasing energy. This model is insensitive to laser intensity for typical experimental conditions, ~ 1 mW laser power in a microprobe apparatus, as is observed in experiment.

This model evaluated with $R_0 = 37.5$ nm in dipole-dipole FRET coupling gives the best fit for the decreased Stokes shifts in the hybrids seen in Fig S2, with good qualitative matching to experiment, and the difference in Stokes shifts as seen in Fig. 3. The results of Ref. 29 suggest that at these very small separations, the dependence could be different due to the importance of quadrupole terms. Using Fig. 6 in Ref. 29, this inclusion leads to

$$\gamma_{\text{coupling}}(r, \rho, R) = \gamma_{\text{rad}}(r)[R'_0/(r + \rho + R)]^{5.6} \quad (9)$$

for the FRET rate. The model predictions are essentially the unchanged, with $R'_0 = 32.1$ nm (Fig. S7).

The Electronic State Model

In this model all levels ($i \geq 1$) are excited electronic states that are equally spaced by Δ .

Because of very fast coupling between these states, the levels are in electronic state equilibration at temperature T_e :

$$n_i = n_{i-1} e^{-\Delta/kT_e} \quad (10)$$

The steady-state number of NPs in the excited electronic state is given by:

$$(\alpha I/E_{\text{exc}})n_0 = \sum_{i=1}^{i_{\text{exc}}} n_i \Gamma'_i \quad (11)$$

where

$$\Gamma'_i = \gamma_{\text{nonrad},i}(r) + \gamma_{\text{rad},i}(r) + \gamma_{\text{coupling},i}(r, \rho, R) \quad (12)$$

The steady state in energy balance is given by:

$$(\alpha I)n_0 = \sum_{i=1}^{i_{\text{exc}}} n_i \Gamma'_i E_i + \sum_{i=2}^{i_{\text{exc}}} n_i \gamma^E \quad (13)$$

Although energy relaxation does not determine the population distribution in this model, it still is an important route of energy loss.

Equations 11 and 13 are solved to give T_e and n_1 . Since T_e usually exceeds room temperature, adding thermal interactions with a bath at ambient temperature is not needed. The

PL spectra are then determined using Eqs. 1 and 11. The spacing between levels 1 and i_{abs} accounts for the entire Stokes shift.

This electronic state model does not reproduce the observed NP or hybrid Stokes shifts, independent of level spacing, and it is sensitive to laser wavelength and intensity. Under common experimental conditions, in this model PL from level 1 is not very important even when all excited states have the same radiative decay rate (and are “bright” states), and so explicitly making it a dark state, with a long radiative lifetime, would not substantially change the predicted PL.

B. Discussion of the Model Results

With $f = 0.5$, the phonon model reproduces the radius-dependent Stokes shifts in unbound NPs well (Fig. S2a) and the decrease in the Stokes shift in the hybrids with smaller NP radius in the hybrids fairly well (Fig. S2b), along with the increase in the Stokes shift difference with smaller NP radius (Fig. 3). This model uses published decay rates, however with energy relaxation rates that are enhanced for higher levels, and FRET from the NP to SWNT in the hybrids. The dipole-limit $1/r^5$ dependence for FRET is used; model predictions do not change when the effect of quadrupolar terms is included (Fig. S7). The model results are insensitive to the energy level spacing, aside from the grainy structure in the variation with particle size that occurs for larger level spacings (Fig. S6) (because all levels are assumed to be separated by the same energy) and that is reinforced by ignoring size and structural inhomogeneity. The observed insensitivity to laser intensity is consistent with model results. The electronic state model does not reproduce the Stokes shift observations, independent of level spacing, and is also sensitive to laser intensity and wavelength.

The phonon model demonstrates the plausibility of the hot luminescence explanation of

the decreased Stokes shifts in the hybrids. The key features of this model are that it is a non-equilibrium, steady-state treatment that is strongly affected by the relative relaxation rates, including that of FRET from the NP to the SWNT. This conclusion does not negate the potential importance of the bright/dark electronic state model of PL from unbound NPs.

C. Relation to Previous Work

Previously, very small decreases in the PL Stokes shifts in hybrids of nanoparticles attached to the walls of SWNTs or nanowires relative to those for unbound nanoparticles were reported⁵. These shifts have usually been attributed to charge transfer, but in some cases to FRET. The much larger shifts seen here may be due to more rapid coupling. A recent study of coupling from a single CdSe NP to the end of a single SWNT suggested coupling by FRET (with a $1/r^6$ dependence for that geometry) and no charge transfer (implied by the lack of change in PL blinking when the NP and SWNT are brought in contact, as is expected for CdSe/ZnS NPs)³¹.

V. Conclusions

Hybrid materials of CdSe nanoparticles and SWNTs are found to photoluminesce with an anomalous, decreased Stokes shift. We have shown that Förster resonance energy transfer from the nanoparticles to semiconductor SWNTs likely leads to this early-stage snapshot of CdSe nanoparticle PL. The observation of this hot luminescence suggests that intra-hybrid coupling may efficiently transfer excitation energy before significant energy relaxation, which would be beneficial for efficient photovoltaics. The dependence of the effect on the type of SWNT indicates a highly sensitive optoelectronic coupling between CdSe nanoparticles and SWNTs, which could be important to future study and applications of these materials. Further investigation is underway using ultrafast optical spectroscopy with better time resolution than that used here and

well-characterized SWNTs in device geometries. SWNT fluorescence should be enhanced due to this FRET. If FRET indeed dominates NP relaxation, it may be important to separate the induced excitons in the SWNT.

The authors thank Louis Brus for valuable discussions. This work was supported primarily by the MRSEC program of the National Science Foundation (DMR-0213574), the NSEC program of the NSF (CHE-0641523), the EFRC program of DoE (DE-SC0001085), and by the New York State Office of Science, Technology, and Academic Research (NYSTAR). Use of the Center for Functional Nanomaterials at Brookhaven National Laboratory, was supported by the U.S. Department of Energy, Office of Science, Office of Basic Energy Sciences, under Contract No. DE-AC02-98CH10886.

References

- 1 N. Cho, K. R. Choudhury, R. B. Thapa, Y. Sahoo, T. Ohulchanskyy, A. N. Cartwright, K. S.
2 Lee, and P. N. Prasad, *Adv. Mater.* **19**, 232 (2007).
3 C. Engtrakul, et al., *J. Phys. Chem. B* **110**, 25153 (2006).
4 S. Banerjee and S. S. Wong, *Chem. Commun.*, 1866 (2004).
5 F. S. Li, D. I. Son, T. W. Kim, E. Ryu, and S. Kim, *Nanotechnol.* **20**, 085202 (2009).
6 L. Hu, Y. L. Zhao, K. Ryu, C. Zhou, J. F. Stoddart, and G. Gruner, *Adv. Mater.* **20**, 939 (2008).
7 I. Robel, B. A. Bunker, and P. V. Kamat, *Adv. Mater.* **17**, 2458 (2005).
8 B. H. Juarez, M. Meyns, A. Chanaewa, Y. X. Cai, C. Klinke, and H. Weller, *J. Am. Chem. Soc.*
9 **130**, 15282 (2008).
10 C. G. Lu, A. Akey, W. Wang, and I. P. Herman, *J. Am. Chem. Soc.* **131**, 3446 (2009).
11 Q. Li, B. Sun, I. A. Kinloch, D. Zhi, H. Sirringhaus, and A. H. Windle, *Chem. Mater.* **18**, 164
12 (2006).
13 M. D. Garrett, A. D. Dukes, J. R. McBride, N. J. Smith, S. J. Pennycook, and S. J. Rosenthal, *J.*
14 *Phys. Chem. C* **112**, 12736 (2008).
15 S. M. Liu, H. Q. Guo, Z. H. Zhang, R. Li, W. Chen, and Z. G. Wang, *Physica E* **8**, 174 (2000).
16 A. L. Efros, M. Rosen, M. Kuno, M. Nirmal, D. J. Norris, and M. Bawendi, *Phys. Rev. B* **54**,
17 4843 (1996).
18 M. Nirmal, C. B. Murray, and M. G. Bawendi, *Phys. Rev. B* **50**, 2293 (1994).
19 M. Kuno, J. K. Lee, B. O. Dabbousi, F. V. Mikulec, and M. G. Bawendi, *J. Chem. Phys.* **106**,
20 9869 (1997).
21 M. S. Dresselhaus, G. Dresselhaus, R. Saito, and A. Jorio, *Physics Reports* **409**, 47 (2005).
22 M. S. Arnold, A. A. Green, J. F. Hulvat, S. I. Stupp, and M. C. Hersam, *Nature Nanotech.* **1**, 60
23 (2006).
24 A. J. Nozik, *Ann. Rev. Phys. Chem.* **52**, 193 (2001).
25 V. I. Klimov, *J. Phys. Chem. B* **104**, 6112 (2000).
26 S. A. Crooker, J. A. Hollingsworth, S. Tretiak, and V. I. Klimov, *Phys. Rev. Lett.* **89**, 186802
27 (2002).
28 D. F. Underwood, T. Kippeny, and S. J. Rosenthal, *J. Phys. Chem. B* **105**, 436 (2001).
29 A. Javier, D. Magana, T. Jennings, and G. F. Strouse, *Appl. Phys. Lett.* **83**, 1423 (2003).
30 X. Y. Wang, L. H. Qu, J. Y. Zhang, X. G. Peng, and M. Xiao, *Nano Lett.* **3**, 1103 (2003).
31 M. Califano, A. Franceschetti, and A. Zunger, *Nano Lett.* **5**, 2360 (2005).
32 J. Z. Zhang, *Acc. Chem. Res.* **30**, 423 (1997).
33 D. M. Mittleman, R. W. Schoenlein, J. J. Shiang, V. L. Colvin, A. P. Alivisatos, and C. V. Shank,
Phys. Rev. B **49**, 14435 (1994).
T. J. Liptay, L. F. Marshall, P. S. Rao, R. J. Ram, and M. G. Bawendi, *Phys. Rev. B* **76**, 155314
(2007).
D. J. Norris and M. G. Bawendi, *J. Chem. Phys.* **103**, 5260 (1995).
P. L. Hernandez-Martinez and A. O. Govorov, *Phys. Rev. B* **78**, 035314 (2008).
R. S. Swathi and K. L. Sebastian, *J. Chem. Phys.* **132**, 104502 (2010).
Z. Chen, S. Berciaud, C. Nuckolls, T. F. Heinz, and L. E. Brus, *ACS Nano* **4**, 2964 (2010).
E. Shafran, B. D. Mangum, and J. M. Gerton, *Nano Lett.* **10**, 4049 (2010).
M. Achermann, M. A. Petruska, S. A. Crooker, and V. I. Klimov, *J. Phys. Chem. B* **107**, 13782
(2003).
F. Buonocore, F. Trani, D. Ninno, A. Di Matteo, G. Cantele, and G. Iadonisi, *Nanotechnol.* **19**,
025711 (2008).

Figure captions

Figure 1. HRTEM micrograph showing CdSe NP/HiPCO SWNT hybrids. The CdSe NPs have an average radius of 2.5 nm. The image was taken at 80 kV accelerating voltage using the aberration corrected JEOL2200MCO TEM. No preferential alignment of the nanoparticle lattice relative to the SWNT is observed.

Figure 2. (a) Photoluminescence from 1.4 nm radius CdSe NPs and HiPCO-SWNT hybrids, and absorbance of NPs. The Stokes shift of the unbound NPs is 158 meV, while that of the hybrids is 8 meV. (b) Photoluminescence from 3.4 nm radius CdSe NPs and HiPCO-SWNT hybrids, and absorbance of NPs. The Stokes shift of the unbound NPs is 60 meV, while that of the hybrids is 50 meV. In both parts, the hybrid PL also shows resonant SWNT Raman scattering peaks¹⁵, indicated by *.

Figure 3. Difference in Stokes shifts between unbound CdSe NPs and HiPCO-SWNT hybrids versus NP radius. The experimental data points are shown, along with phonon model results (with $f=0.5$, $\Delta=1$ meV, and enhanced energy relaxation at higher levels).

Figure 4. Photoluminescence from CdSe/ZnS core-shell NPs and HiPCO-SWNT hybrids, and absorbance of NPs. The core CdSe NPs are 1.8 nm in radius; the ZnS shell is 1.5 nm thick. The Stokes shift of core-shell NPs is 36 meV; for hybrids it is 13 meV. Excitation is at 514.5 nm. * indicates SWNT resonant Raman scattering peaks.

Figure 5. Ultrafast photoluminescence from 1.7 nm radius CdSe NPs and HiPCO-SWNT hybrids. Excitation is at 455 nm and collection is at 577 nm (the peak of the NP PL signal in cw

measurement). * denotes a data artifact arising from the instrument at 17 ns, in both NP and hybrid signals.

Figure 6. Photoluminescence from 2.2 nm radius CdSe NPs and of hybrids made with enriched semiconducting or metallic arc-discharge SWNTs, and NP absorbance. The Stokes shift of the unbound NPs is 46 meV and that of the semiconducting SWNT-hybrid is 22 meV. The Stokes shift of the metallic SWNT-hybrids is 7 meV. * indicates SWNT resonant Raman scattering peaks.

Figure 7. Schematic of the model, with relaxation routes explicitly depicted for $i = 3$. This is explicitly for the phonon model; the schematic for the electronic state model is similar.

Figure 1

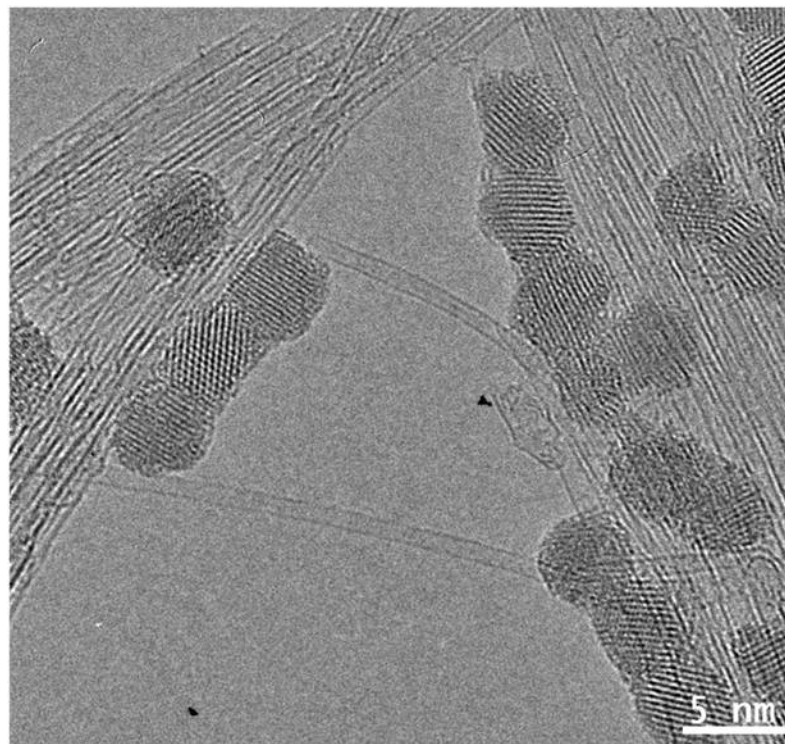


Figure 2

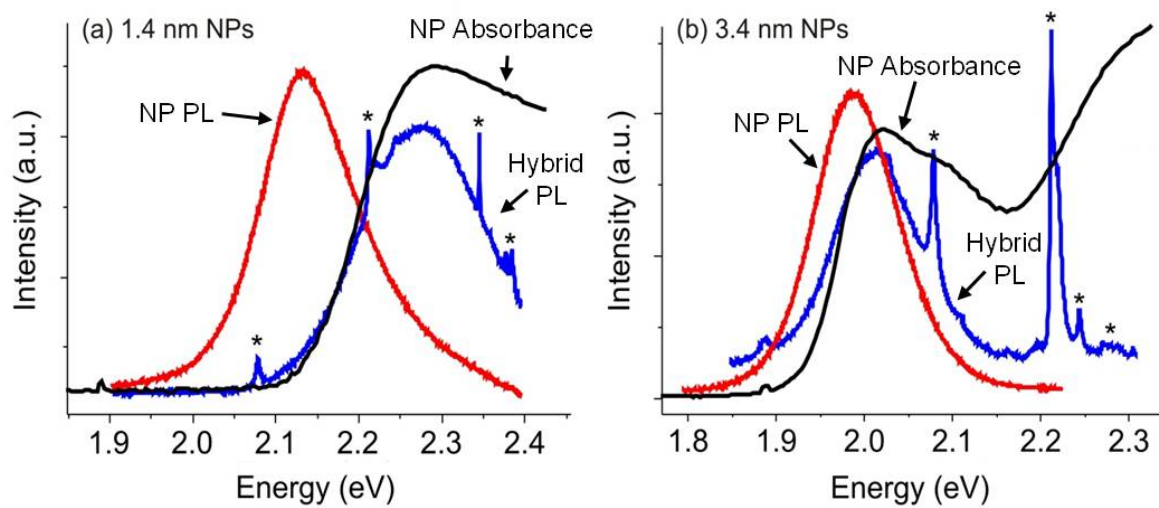


Figure 3

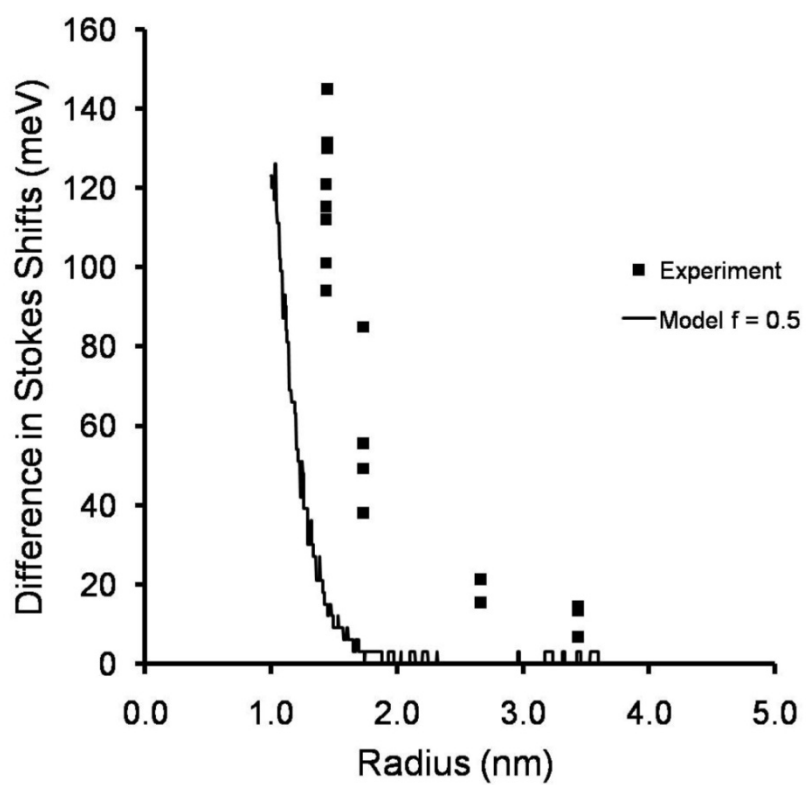


Figure 4

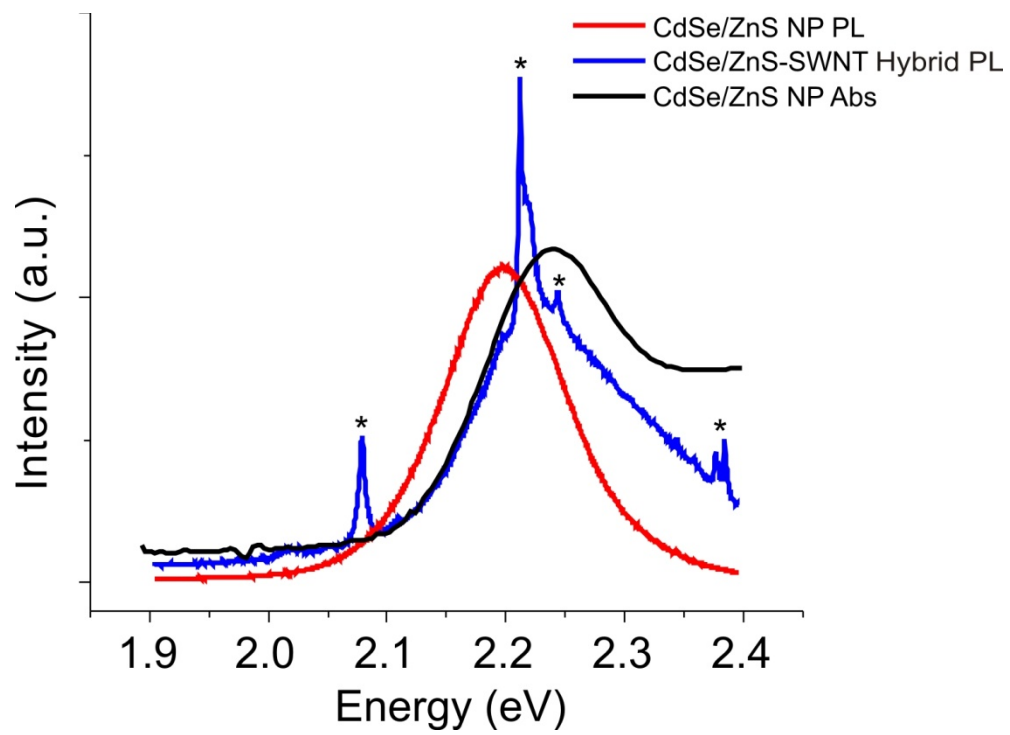


Figure 5

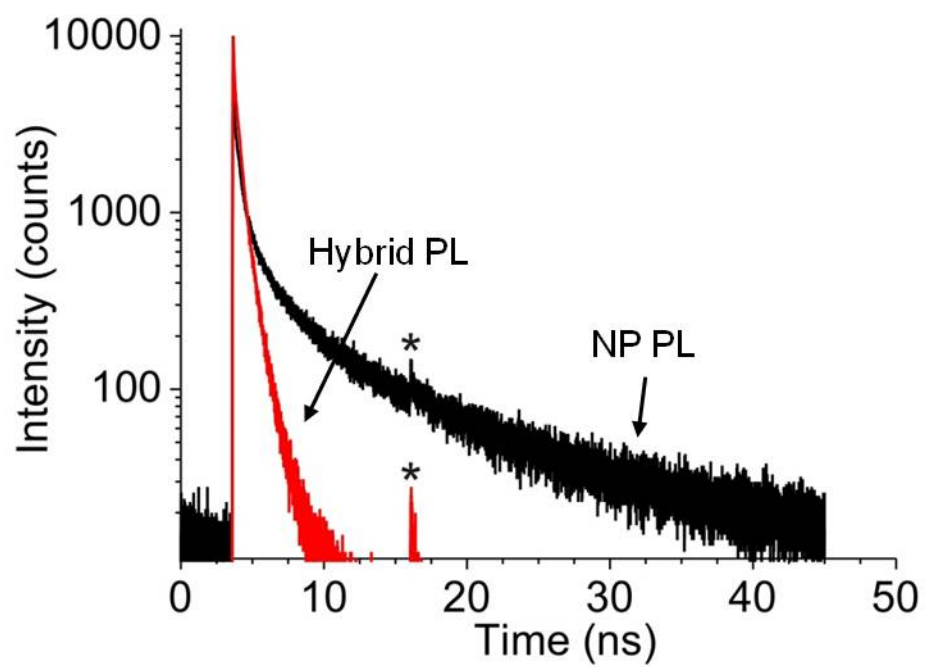


Figure 6

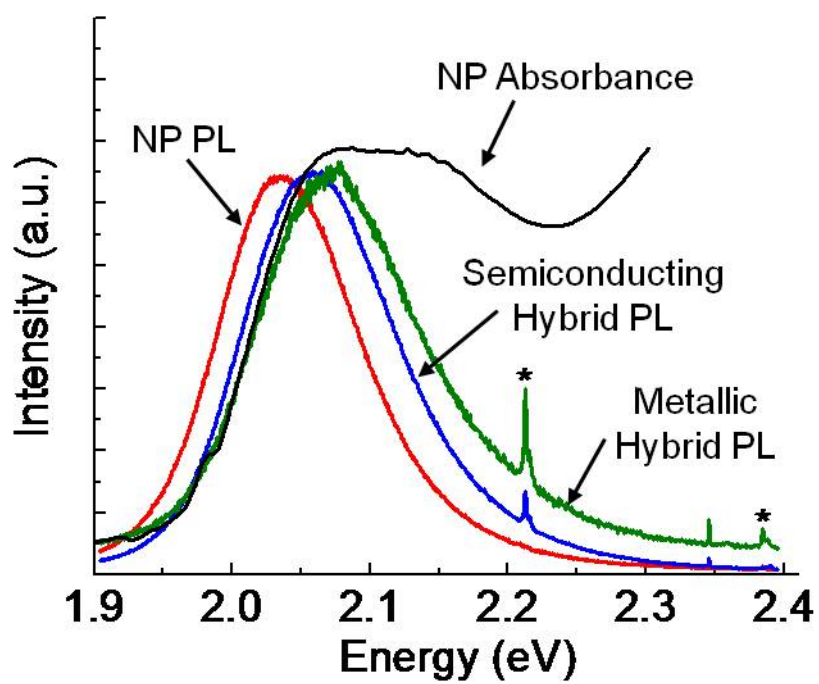


Figure 7

